





RESEARCH ARTICLE | APRIL 19 2024

Magnetic properties of $\text{Fe}_{56}\text{Pd}_{44-x}\text{Gd}_x$ thin films

Mohamed Abdenmour Sahari ; Elena Sonia Olivetti ; Alessandro Magni ; Gianluca Fiore; Mokhtar Boudissa; Paola Tiberto; Saida Bahamida; Marco Coisson 



J. Appl. Phys. 135, 153903 (2024)

<https://doi.org/10.1063/5.0197933>



Articles You May Be Interested In

Disordered to ordered phase transformation: Correlation between microstructure and magnetic properties in Fe–Pd thin films

J. Appl. Phys. (March 2022)

Origin of magnetic anisotropy, role of induced magnetic moment, and all-optical magnetization switching for $\text{Co}_{100-x}\text{Gd}_x/\text{Pt}$ multilayers

APL Mater. (June 2021)

Theory of magnetization of n-type $\text{Pb}_{1-x}\text{Gd}_x\text{S}$ diluted magnetic semiconductor

AIP Conference Proceedings (February 2021)



Journal of Applied Physics

Special Topics Open
for Submissions

[Learn More](#)

Magnetic properties of $\text{Fe}_{56}\text{Pd}_{44-x}\text{Gd}_x$ thin films

Cite as: J. Appl. Phys. 135, 153903 (2024); doi: 10.1063/5.0197933

Submitted: 15 January 2024 · Accepted: 22 March 2024 ·

Published Online: 19 April 2024



Mohamed Abdennour Sahari,^{1,a)} Elena Sonia Olivetti,² Alessandro Magni,² Gianluca Fiore,³ Mokhtar Boudissa,⁴ Paola Tiberto,² Saida Bahamida,⁵ and Marco Coisson²

AFFILIATIONS

¹Research Laboratory: IRME—Department of Physics, University of Boumerdes, Boumerdes, Algeria

²Advanced Materials and Life Sciences Division, INRIM, strada delle Cacce 91, 10135 Torino, TO, Italy

³Dipartimento di Chimica e Centro Interdipartimentale NIS (Nanostructured Surfaces and Interfaces), Università di Torino, Via Pietro Giuria 7, 10125 Torino, Italy

⁴ENMC Laboratory, Department of Physics, Faculty of Sciences, University Ferhat Abbas, Setif 19000, Algeria

⁵Research Unit UR-MPE, University of Boumerdes, 1 Avenue de l'Indépendance, Boumerdes 35000, Algeria

^{a)}Author to whom correspondence should be addressed: m.sahari@univ-boumerdes.dz

ABSTRACT

In this paper, we have studied the effect on the structure and magnetic properties of partial Pd substitution by Gd in Fe–Pd thin films of nominal composition $\text{Fe}_{56}\text{Pd}_{44-x}\text{Gd}_x$ ($x = 1, 3, 5,$ and 7), deposited onto Si(100) and Si(100)/SiO₂ substrates by thermal evaporation. Several techniques contribute to the characterization of their microstructure and magnetic properties, such as x-ray diffraction (XRD), scanning electron microscopy, alternating gradient field magnetometry, and magnetic force microscopy (MFM). X-ray diffraction shows that the as-deposited films are either amorphous or contain a disordered FePd phase, depending on the film thickness. The transformation of disordered fcc-FePd into ordered fct-FePd has been induced by a heat treatment at 530 °C for 4 h. The addition of gadolinium leads to a reduction in the coercivity as a consequence of the emergence of soft phases and of the progressive reduction of the fct-FePd phase, which is primarily responsible for the observed maze magnetic domains. The exchange coupling between the soft phase and the hard fct-FePd phase is demonstrated by first-order reversal curves (FORCs).

© 2024 Author(s). All article content, except where otherwise noted, is licensed under a Creative Commons Attribution (CC BY) license (<https://creativecommons.org/licenses/by/4.0/>). <https://doi.org/10.1063/5.0197933>

I. INTRODUCTION

The addition of rare earth elements (REEs) to binary alloys has become attractive for many different reasons,¹ such as tailoring their magnetic properties to match the needs of many different applications: permanent magnets, magnetostrictive detectors, magnetocaloric materials, magnetoresistance, etc.^{2,3} The properties obtained are normally adequate for their respective applications in systems with REE. The most high-performance permanent magnets incorporate rare-earth elements such as (Pr, Nd, Sm, Tb, or Dy),⁴ which can enhance the Curie temperature (T_c) and the magnetic anisotropy, as shown by numerous studies on permanent magnets and magneto-optical media.^{5–7} Recently, Gd has been considered more suitable compared to other rare earth elements (Nd, Tb, Pr, and Dy): in fact, it is more abundant than these elements in natural resources, and it is much less sensitive to oxidation than light REE. Moreover, since Gd is much cheaper than Nd, Tb, Pr, and Dy, it

may become viable to reduce the cost of magnets by replacing these elements.⁸ In addition, for some alloys, such as Fe–Pd, even if there is not a rare earth, the replacement of Pd, a precious metal, with less costly materials may be desirable. It would be interesting to check whether the substitution of some of it by gadolinium could lead to different properties than the conventional ferromagnetic Fe–Pd system,^{9–13} which, depending on its composition and crystalline phase,^{14–17} can show the shape memory effect¹⁸ or display particular magnetic properties useful for many applications such as hydrogen adsorption,^{19,20} biomedical engineering,²¹ magnetic data storage,¹⁴ and other special applications.^{22–25} In particular, around the equiatomic composition, the Fe–Pd alloy can develop the tetragonal L1₀-FePd phase, an ordered phase of the AuCu type, which shows hard magnetic properties. The strong uniaxial magneto-crystalline anisotropy of this intermetallic compound is exploited for perpendicular magnetic recording.²⁶ As we mentioned before, the addition of Gd to this binary system could enrich the magnetic behavior of

11 November 2024 09:37:28

the Fe–Pd system, for example, affecting coercivity, saturation magnetization, and magnetocrystalline anisotropy, which are important and essential properties for magnetic applications,⁴ thanks to the variety of phases that may be formed, also as a consequence of thermal treatments. As a result, the already rich magnetic behavior of the Fe–Pd system may benefit for the equally rich behavior of the Fe–Gd one.²⁷ By developing a ternary Fe–Pd–Gd compound, it is, therefore, hoped that a more complex and varied microstructure can develop, affecting the magnetic properties of the Fe–Pd system. It has to be pointed out that even though many reports indicate an improvement of the hard magnetic properties of ferromagnetic materials when REEs are added, the complexity of the system does not ensure successful results, and their weakening is also possible,^{28–31} for example, through antiferromagnetic couplings between Fe 3d and Gd 4f magnetic moments that can also lead to a decrease in saturation magnetization (Ms). Since the investigation of the Fe–Pd–Gd alloys is nowadays almost unexplored, in this paper, we have studied the effect of partial Pd replacement by Gd in Fe–Pd thin films evaporated onto Si(100) and Si(100)/SiO₂ substrates to understand how the microstructure of this ternary system compares with that of the known Fe–Pd alloy, and consequently, how the magnetic properties are affected. An in-depth investigation of the structural and magnetic properties has, therefore, been performed on both as-prepared and thermally annealed samples, with the aim of helping clarify the magnetic properties of the so far almost unexplored Fe–Pd–Gd ternary system.

II. EXPERIMENTAL METHODS

The different Fe₅₆Pd_{44-x}Gd_x alloys used in this work were prepared by vacuum evaporation on a polycrystalline silicon substrate Si(100) and on Si/SiO₂, which could lead to different properties of the samples. The main difference in the substrates is the thickness of the oxide layer on the top of the Si(100), i.e., for the Si substrate, the oxide layer is just a few nm thick since it comes from the natural oxidation of the wafer exposed to air, which is a self-limiting process, whereas for Si/SiO₂ substrate, the oxide layer is thicker (500 nm) because the oxidation has been thermally promoted. For preparation, pure elemental powders (Gd: 99.9%, Fe: 99.9%, and Pd: 99.9%) were used. All elements were disposed in a tungsten crucible, which, in turn, was placed in the chamber of the evaporator under a base pressure of 10⁻⁷ mbar. In this study, four films were made from sufficient amounts of gadolinium to obtain films having nominal compositions Fe₅₆Pd₄₃Gd₁, Fe₅₆Pd₄₁Gd₃, Fe₅₆Pd₃₉Gd₅, and Fe₅₆Pd₃₇Gd₇. After deposition, the films' thickness was estimated from the fringe position of an x-ray reflectivity curve and turned out to be, respectively, 100, 61, 25, and 12 nm for the four compositions; this thickness reduction was not expected, as the total amounts of powders placed in the crucibles were supposed to result in films all having approximately the same thickness. Moreover, to verify the chemical composition of the films, x-ray energy scattering (EDS) analysis was exploited; however, the amount of Gd in the samples was too little, resulting in a signal below the detection limit. Indeed, other authors have experienced difficulties, if not impossibility, in detecting Gd in ternary systems with Gd content comparable to ours.^{32,33} Even though with the current results, it is not possible to assess how much Gd is present

in the samples, and where it finds its place in the microstructure, we will demonstrate that we can still observe an evolution of the magnetic properties in samples with different nominal Gd content, letting us indirectly infer its effects on microstructure and related magnetic properties.

Even though EDS was not sensitive enough to detect Gd, the relative amounts of both Fe and Pd were still measurable, and we have plotted the evolution of the experimental Pd/Fe ratio as a function of the nominal ratio as obtained by EDS analysis. The result is shown in Fig. 1, a black curve, which gives an illustration of the substitution of some Pd with Gd. The experimental Pd/Fe ratio follows the expected (nominal) trend, even though there are clearly some discrepancies: at low Gd content (high Pd/Fe ratio), the experimental ratio is slightly below the nominal value; in principle, this could be due to either a larger than expected Gd content or to a lower than expected Pd amount with respect to Fe. However, as the Gd content increases, the discrepancy becomes larger, indicating that either more Gd or less Pd was evaporated than expected. The anomaly in the samples' composition is accompanied by the unexpected thickness reduction with Gd content increase, as discussed above. Apparently, when the Gd amount is increased in the crucibles, less material turns out to be deposited onto the substrates. Whatever mechanism is happening during the deposition process, the two discrepancies (thickness reduction and Pd depletion) seem to be correlated. With this important remark in mind, we will, nonetheless, label the samples in the following with their nominal Gd content (i.e., 1, 3, 5, and 7%) for simplicity.

It is worth commenting that the evaporation of rare earth elements is a difficult process, involving only a limited amount of material, which cannot be fed into the evaporator without breaking the void. Therefore, if the final sample thickness is less than expected as in our case for the specimens with higher Gd content,

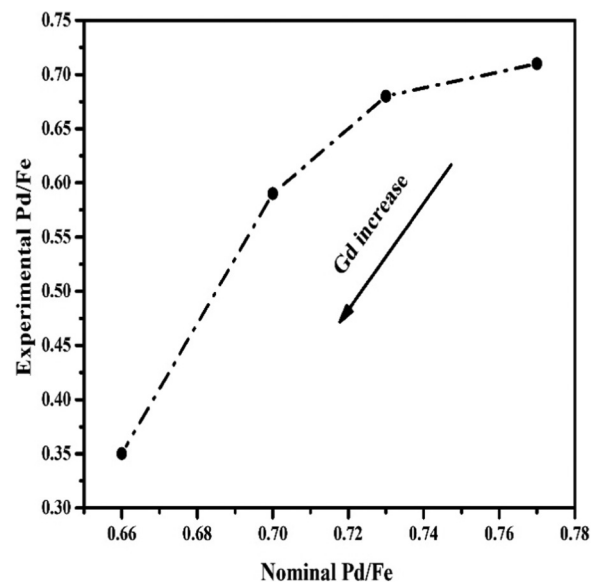


FIG. 1. Evolution of experimental Pd/Fe ratio as a function of theoretical ratio.

11 November 2024 09:37:28

there is no obvious path to obtain higher thickness by increasing the amount of evaporated powders and deposition time.

To induce phase transformations in the films, annealing treatment has been done for all samples in a furnace under vacuum (base pressure 2×10^{-6} mbar) at 530 °C for 4 h. All as-prepared and annealed samples were characterized with an x-ray diffractometer (PANalytical X'pert pro) using a $\text{CuK}\alpha$ radiation source ($\lambda = 0.15406$ nm), to explore their structural properties. To reduce the substrate contribution in the measured x-ray diffraction (XRD) diffraction patterns, the grazing incidence configuration has been adopted, with the angle of incidence of the x-ray beam on the sample surface fixed at 1° . The average scattering domain (D) is estimated according to Bragg's law and Scherrer's formula.³⁴

In addition, the morphology of all samples was investigated by means of scanning electron microscopy (SEM) (SEM—FEI Inspect-F) at 10 kx magnification and acceleration voltage fixed to 20 kV, exploiting backscattered electron imaging (BSE), which offers a better visual contrast between phases based on their electron density.³⁵ Finally, the magnetic characteristics of all films were determined at room temperature with an alternating gradient field magnetometer (AGFM, PMC 2900) by applying a magnetic field parallel to the surface of the films. Besides hysteresis loops, first-order reversal curves (FORCs) were also measured by the AGFM to obtain a more detailed description of the magnetization process in the films and to study the coexistence and interactions of different magnetic phases. Furthermore, the magnetic domain structures have been observed by atomic and magnetic force

microscopy (MFM, Bruker Multimode V Nanoscope 8), on both as-prepared and annealed samples, at their in-plane magnetic remanence, using Co-coated Si tips magnetized along their axis (i.e., perpendicularly to the film surface).

III. RESULTS AND DISCUSSION

A. As-deposited films

1. Microstructure properties

All the as-deposited samples $\text{Fe}_{56}\text{Pd}_{44-x}\text{Gd}_x$ show a smooth and flat surface with no visible morphological details even at high magnification, as shown in Figs. 2(a) and 2(b) for Gd1, as an example.

The x-ray diffractograms of $\text{Fe}_{56}\text{Pd}_{44-x}\text{Gd}_x$ samples deposited on Si and SiO_2 substrates are shown in Fig. 3. Peaks marked with (+) are Laue spots due to diffraction from the white radiation from the single crystal substrate in the asymmetric geometry of measurement.³⁶ The Gd1 and Gd3 as-deposited samples are polycrystalline, composed of a disordered fcc-FePd phase, while Gd5 is in an amorphous state. For Gd7 films, because of their reduced thickness causing the overall low signal, definitive conclusions cannot be drawn about the phases present; however, since no reflections are visible, the amorphous state can be considered probable.

An amorphization with increasing Gd concentration was already observed in Ref. 37 and also in the Fe-Gd²⁸ and in the Gd-Co-Fe-Al³⁸ systems. Table I (left part) summarizes the phases

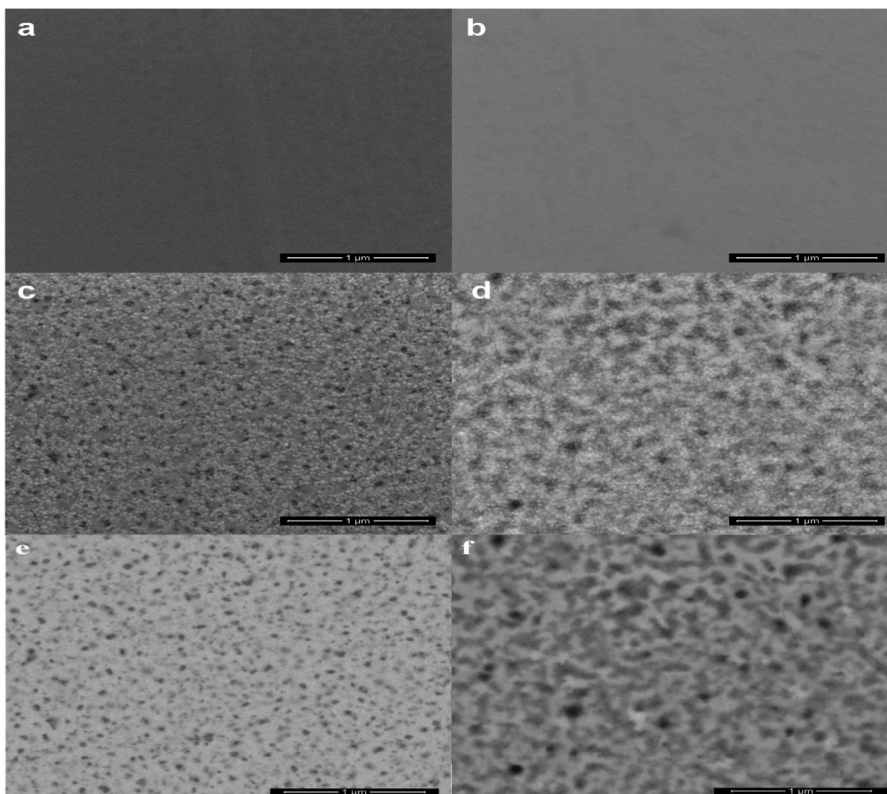


FIG. 2. SEM secondary electron images of $\text{Fe}_{56}\text{Pd}_{43}\text{Gd}_1$ thin films: (a) as-prepared film on the Si substrate, (b) as-prepared film on the SiO_2 substrate, (c) annealed film on the Si substrate, (d) annealed film on the SiO_2 substrate, and (e) SEM backscattered electrons' image of the annealed film: (e) on the Si substrate and (f) on the SiO_2 substrate.

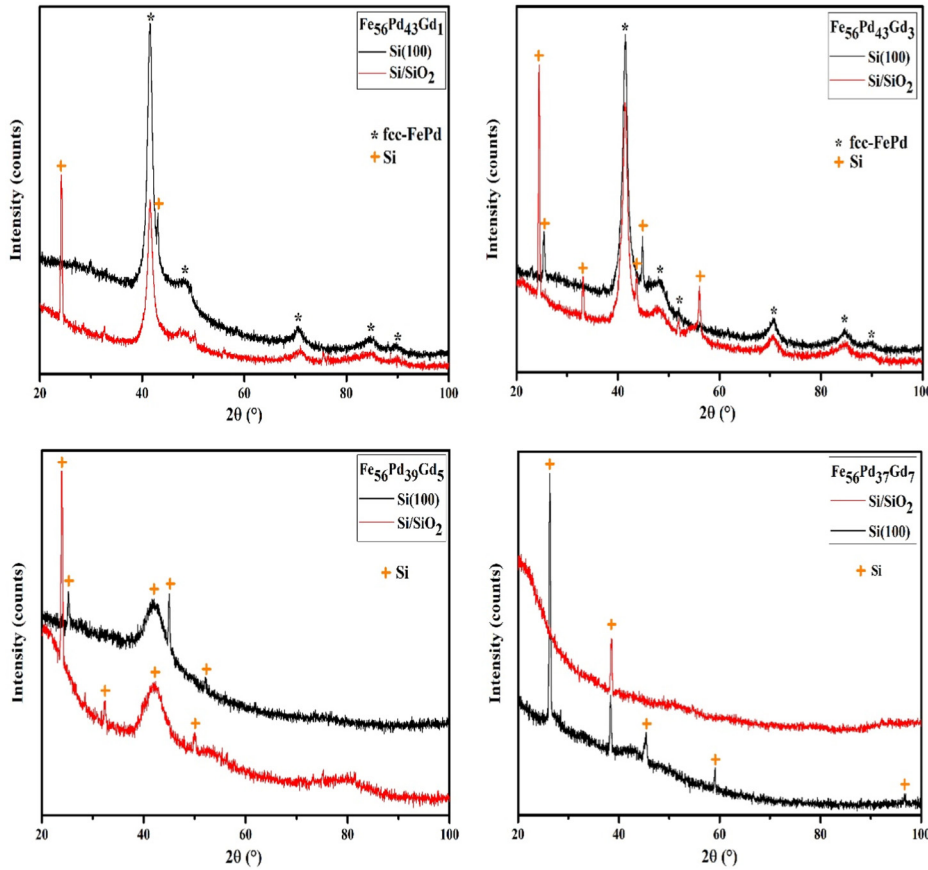


FIG. 3. X-ray diffraction patterns of the as-prepared $\text{Fe}_{56}\text{Pd}_{44-x}\text{Gd}_x$ thin films on the Si and SiO_2 substrates.

present in the different as-deposited samples, as detected by the x-ray analysis.

2. Magnetic properties

Hysteresis loops at room temperature, obtained from AGFM measurements with in-plane magnetic field, are reported in Fig. 4.

As clearly shown, the shape of the hysteresis loops for all the samples is narrow and curved, confirming that all as-deposited samples are soft ferromagnets.

The differences in H_c values (listed in Table II together with the average scattering domain size obtained from XRD data) are minimal and difficult to attribute to specific causes, as they might be related to the presence of the fcc phase in different amounts as

TABLE I. The different phases present in the as-deposited and annealed $\text{Fe}_{56}\text{Pd}_{44-x}\text{Gd}_x$ films. (The question mark shown in the table means “possible,” in the sense that it seems reasonable to assign the observed reflections to that phase but, owing to the low intensity of peaks and/or to the overall low signal due to the small thickness of the film, no definitive conclusions can be drawn about the phase actual presence).

Samples	As-deposited		Annealed at 530 °C	
	Si	SiO_2	Si	SiO_2
Gd1 ($\text{Fe}_{56}\text{Pd}_{43}\text{Gd}_1$)	fcc-FePd	fcc-FePd	$L1_0$ FePd α -Fe Pd_2Si	$L1_0$ FePd Fe_3O_4
Gd3 ($\text{Fe}_{56}\text{Pd}_{41}\text{Gd}_3$)	fcc-FePd	fcc-FePd	$L1_0$ FePd α -Fe	$L1_0$ FePd α -Fe
Gd5 ($\text{Fe}_{56}\text{Pd}_{39}\text{Gd}_5$)	Amorphous	Amorphous	$L1_2$ FePd_3 α -Fe	$L1_2$ FePd_3 Fe_3O_4
Gd7 ($\text{Fe}_{56}\text{Pd}_{37}\text{Gd}_7$)	Amorphous (?)	Amorphous (?)	$L1_0$ FePd (?) α -Fe (?)	$L1_2$ FePd_3 (?) Fe_3O_4 (?)

11 November 2024 09:37:28

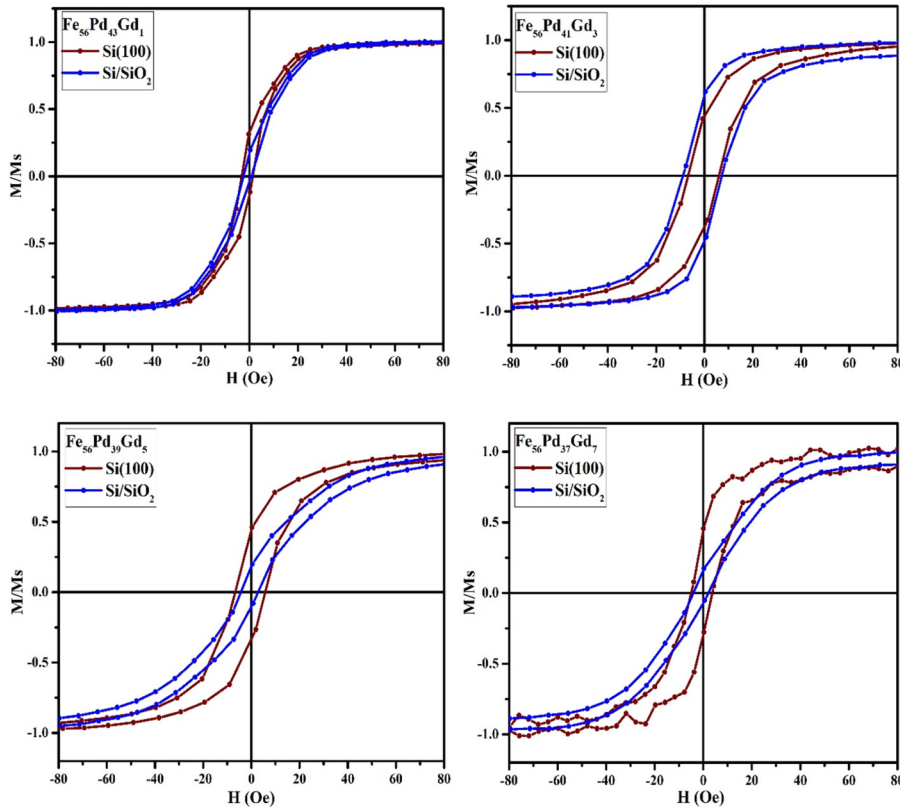


FIG. 4. Magnetic hysteresis loops of the as deposited $\text{Fe}_{56}\text{Pd}_{44-x}\text{Gd}_x$ films deposited on Si and Si/SiO_2 .

well as of defects (grain boundaries, local stresses) and to the different substrates, which induce small fluctuations in the movement of the magnetic domain walls^{39–41} and, therefore, the small variations of H_c . In any case, they qualitatively reflect an expected general, where coercivity should be low at high thickness, where domain wall mobility is high, and at low thickness, where the dominant magnetization reversal process is rotations, with a peak in-between, as it is the case for Gd3 samples.

Figure 5, reporting the MFM images at the in-plane remanence of all the as-deposited films, shows that the samples have a weak magnetic contrast, with some domains and their respective domain walls visible, which we can attribute to the disordered FePd phase whose magnetization local points slightly off the sample plane, following the local random anisotropies.

B. Annealed films

1. Morphology and microstructure

The XRD patterns of the $\text{Fe}_{56}\text{Pd}_{44-x}\text{Gd}_x$ films deposited onto Si and SiO_2 are shown in Fig. 6, and the phases present in the annealed films are anticipated in Table II, right part. The samples can be divided into two groups, the ones in which an $L1_0$ FePd ordered phase developed upon annealing and the ones in which, instead, the annealing treatment promoted the formation of $L1_2$ FePd₃, a different ordered phase, with the cubic structure of the AuCu₃ type. In addition to these main phases, either α -Fe or Fe_3O_4 , were observed depending on the sample. As it will be discussed later, this phase mix has a relevant effect on the films' magnetic properties. In the case of Gd1 and Gd3 films, the main phase

TABLE II. Coercive field (H_c) and scattering domain size (D) values of as-deposited $\text{Fe}_{56}\text{Pd}_{44-x}\text{Gd}_x$ films.

Samples	Si		SiO_2	
	H_c (Oe)	D (nm)	H_c (Oe)	D (nm)
$\text{Fe}_{56}\text{Pd}_{43}\text{Gd}_1$	2.17	9.4	1.62	9.3
$\text{Fe}_{56}\text{Pd}_{41}\text{Gd}_3$	6.39	9.7	8.02	9.8
$\text{Fe}_{56}\text{Pd}_{39}\text{Gd}_5$	6.17	/	3.59	/
$\text{Fe}_{56}\text{Pd}_{37}\text{Gd}_7$	4.37	/	3.11	/

11 November 2024 09:37:28

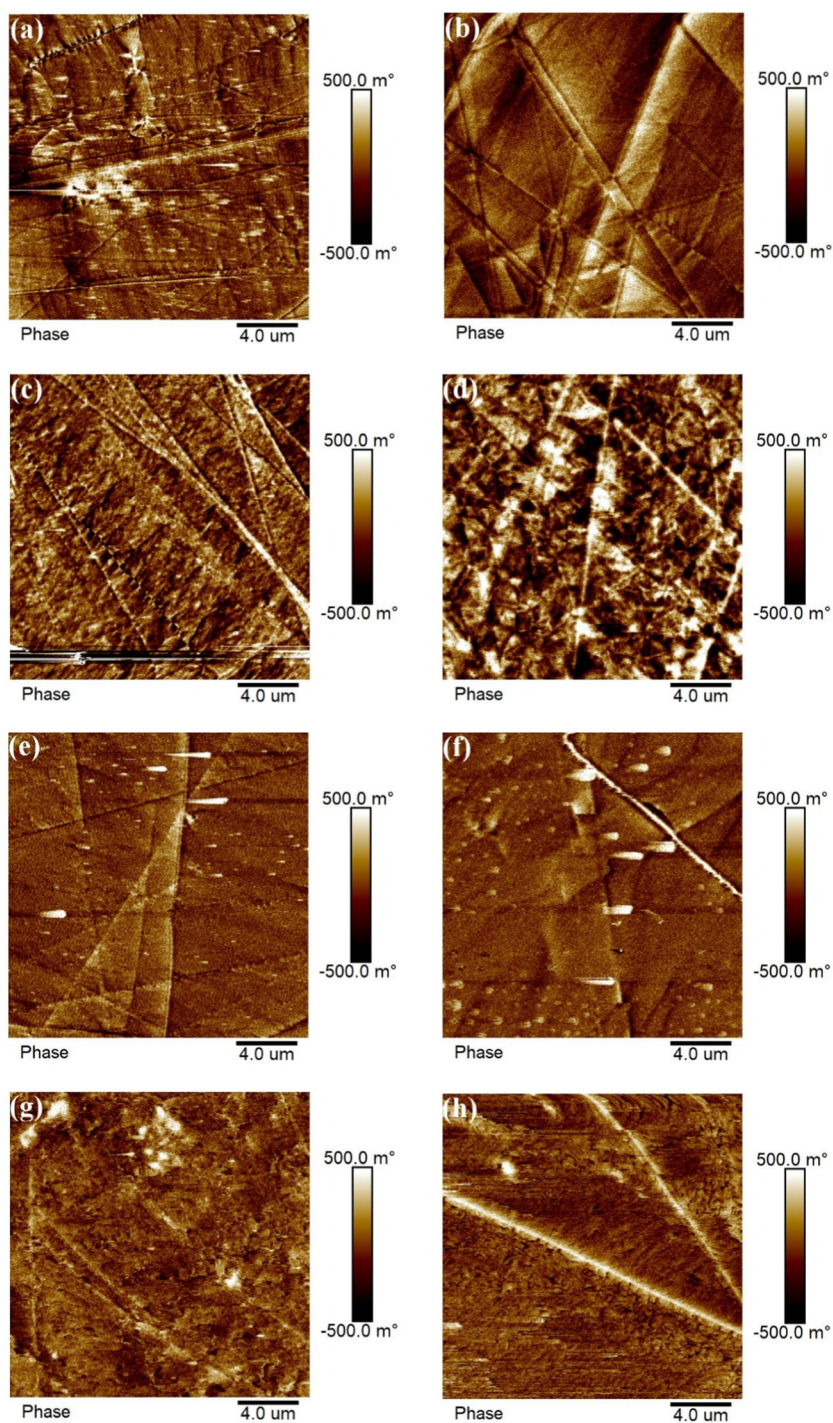


FIG. 5. MFM images of as-deposited $\text{Fe}_{56}\text{Pd}_{44-x}\text{Gd}_x$ films: (a) Gd1/Si; (b) Gd1/SiO₂; (c) Gd3/Si; (d) Gd3/SiO₂; (e) Gd5/Si; (f) Gd5/SiO₂; (g) Gd7/Si; and (h) Gd7/SiO₂.

11 November 2024 09:37:28

is $L1_0$ FePd, regardless of the substrate, while a difference is observed in the secondary phase, being α -Fe in all the cases except Gd1/SiO₂. In addition, for Gd1/Si and Gd3/Si, the XRD pattern shows also several low-intensity peaks that can be ascribed to traces

of Pd₂Si or FeSi₂ phases, which reveal an incipient reaction of the metal film with the substrate material to form silicides, a well-known phenomenon that can occur even at temperatures as low as 200 °C.⁴² These silicides have been observed also in the SEM

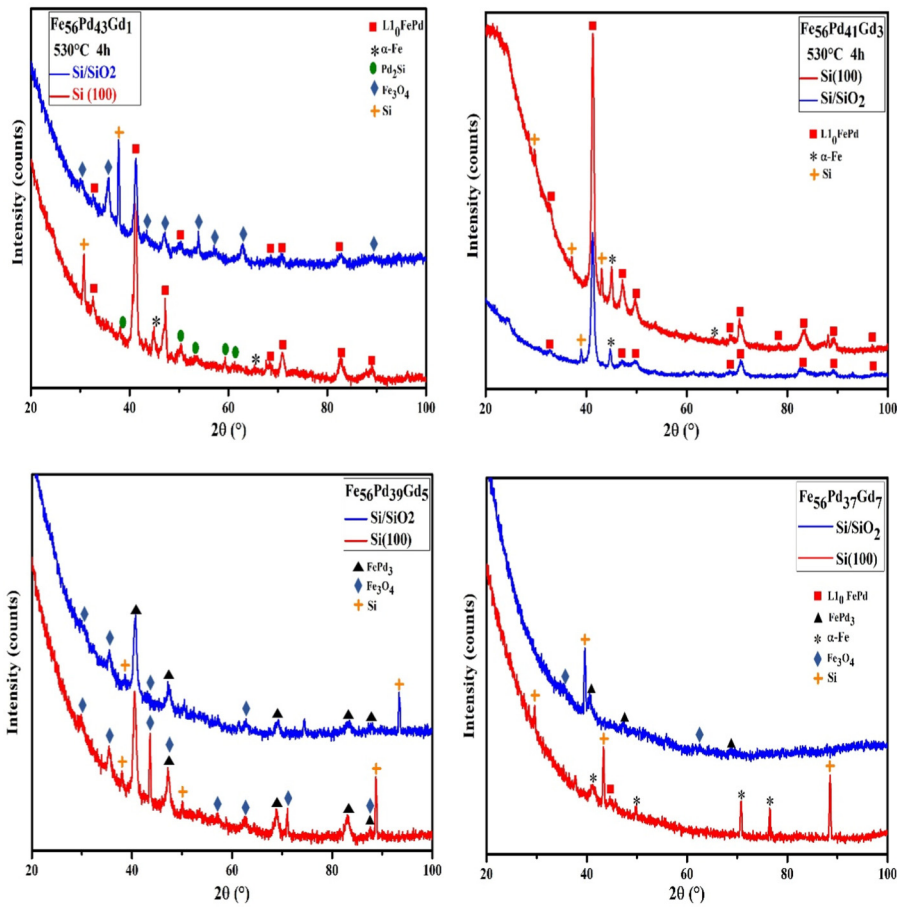


FIG. 6. XRD patterns of $\text{Fe}_{56}\text{Pd}_{44-x}\text{Gd}_x$ annealed films deposited on Si (red line) and SiO_2 (blue line).

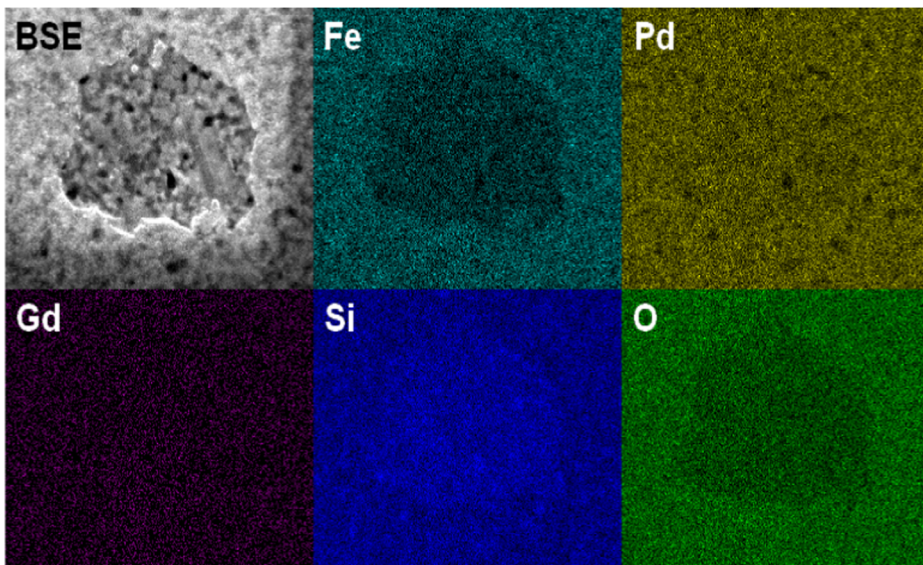


FIG. 7. SEM backscattered electrons image of sample $\text{Fe}_{56}\text{Pd}_{43}\text{Gd}_1$ on SiO_2 and elemental x-ray maps of the area; the characteristic x-ray energies of selected elements (Fe, Pd, Gd, Si, and O) are represented in false colors.

11 November 2024 09:37:28

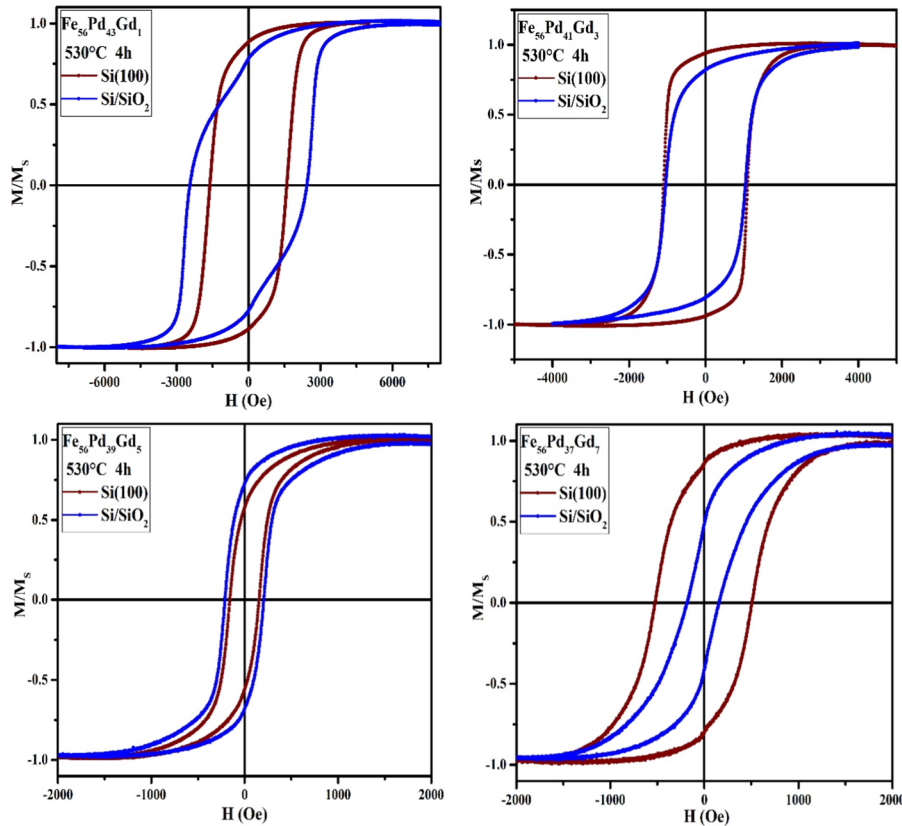


FIG. 8. Room-temperature hysteresis loops of the $\text{Fe}_{56}\text{Pd}_{44-x}\text{Gd}_x$ thin film annealed at $T = 530^\circ\text{C}$ for $t = 4\text{h}$.

pictures as crystal agglomerates occasionally present on some spots of the films surface. For Gd5 films, only reflection corresponding to the $\text{L1}_2\text{-FePd}_3$ phase was observed, accompanied by the ones of Fe_3O_4 . In Gd7 films, only very weak reflections are visible, which are tentatively identified as reported in Table I and in the figure legend; however, as already mentioned about the as-deposited films, phases' identification of Gd₇ film remains uncertain due to the very small thickness of these films and shall be confirmed by magnetic data.

The morphology of each alloy $\text{Fe}_{56}\text{Pd}_{44-x}\text{Gd}_x$ deposited on Si and SiO_2 substrates and subsequently annealed has been studied by SEM along with exploiting backscattered electron (BSE) imaging, which provides better optical contrast between phases based on electron density. Figure 2 (panels c and d) and (panels e and f) shows the secondary electron and backscattered images of the thick solid sample ($\text{Fe}_{56}\text{Pd}_{43}\text{Gd}_1$) deposited on Si and SiO_2 , respectively. Figure 2 (c and d panels) shows the secondary electrons images of the thickest annealed sample ($\text{Fe}_{56}\text{Pd}_{43}\text{Gd}_1$) deposited on Si and SiO_2 , respectively, as an example of the observed morphologies: the samples are no longer flat and featureless as in the as-deposited state but developed a fine-grained morphological contrast, consisting of regions with different shades of gray [Figs. 2(e) and 2(f)]. Such contrasts were also observed in Mg–Al systems enriched with REE,⁴³ and the brighter regions were attributed to phases richer in rare earth, which are heavier and backscatter the electrons more

efficiently. Also in our case, even if attributing each shade of gray to a specific phase is not possible, we can still assume that the brighter regions are richer in Gd.

Figure 7 shows a BSE image coupled with false color EDS elemental maps of a feature observed several times in the Gd1/ SiO_2 sample: the fine-grained morphology observed also in secondary electrons images has a hole that allows us to see an underlying layer with sharper and larger grains. The maps of elemental distribution reveal that the hole is enriched in Si, presumably owing to the reduced thickness of the layer, while on the contrary, the surrounding area is enriched in Fe and O with respect to the hole, suggesting that the fine-grained layer on top of the film is constituted by Fe_3O_4 , whose peaks were also detected in the XRD pattern. Therefore, it is possible to deduce that Fe_3O_4 , where present, constitutes an oxidation layer on the film surface accidentally formed during the annealing treatments.

2. Magnetic properties

Room-temperature in-plane hysteresis loops of the annealed films on Si and SiO_2 together are given in Fig. 8. The shape of the obtained hysteresis loops is characteristic of a ferromagnetic material for all samples independent of the chosen substrate, showing, in all the cases, much harder magnetic properties than for the as-deposited samples. The measured magnetic properties

TABLE III. The coercive field (H_c), the saturation magnetization (M_s), and scattering domain size (D) values of the annealed films.

Alloy	Si(100)			Si/SiO ₂		
	H _c (Oe)	M _s (emu/cm ³)	D(nm) (L1 ₀ FePd)	H _c (Oe)	M _s (emu/cm ³)	D(nm) (L1 ₀ FePd)
Fe ₅₆ Pd ₄₃ Gd ₁	1601	519	49.1	2408	354	33.5
Fe ₅₆ Pd ₄₁ Gd ₃	1093	1233	36.4	1043	711	25.4
Fe ₅₆ Pd ₃₉ Gd ₅	158	220	/	208	287	/
Fe ₅₆ Pd ₃₇ Gd ₇	521	424	10.6	174	194	/
Fe ₅₆ Pd ₄₄		H _c = 1973 Oe ¹⁷			M _s = 1183 emu/cm ³ ¹⁷	

are closely related to the structure and the different phases developed during the annealing of the films and are reported in Tables III and IV.

The presence of the L1₀ phase in the films leads to large coercive fields, whose values will no longer follow a trend with thickness as for the as-deposited samples. In fact, the specimens where the L1₀ phase has been detected in their respective XRD patterns (see Table I and Fig. 6) display the larger hysteresis loops. Sample Fe₅₆Pd₄₃Gd₁ deposited on Si has a lower H_c value (1601 Oe) than the one deposited on SiO₂ (2408 Oe), possibly due to a higher formation of L1₀ FePd in the film deposited on Si/SiO₂; conversely, the saturation magnetization M_s is larger in the films deposited on Si since α-Fe is present (not visible in Fig. 8 since the magnetization data are normalized to saturation for ease of comparison). The sample with 3% of Gd confirms this result, where Gd3/Si and Gd3/SiO₂ display almost the same H_c values but with different M_s values. Both films consist of two phases: L1₀ FePd and α-Fe (see Table I). The difference in M_s values can be related to the soft phase (α-Fe), which may be present in different amounts. Conversely, in Gd₅ samples, only soft phases with comparatively low saturation magnetization are present (L1₂ FePd₃ and Fe₃O₄); thus, the coercive field and saturation magnetization are lower than in the previous films. On the other hand, the gradual and significant decrease of H_c (H_c = 1601–158 Oe for Gd = 1%–5%) and (H_c = 2408–174 Oe) for silicon and silicon oxide, respectively (see Tables III and IV), is correlated to the decrease of L1₀ FePt phase with increasing amount of Gd. This result may also be related to the decrease in the scattering domain size, as obtained by XRD (see Table III), since Zhang *et al.*²⁸ have reported that the coercivity decreases with the reduction in scattering domain size in Fe–Gd thin films. Furthermore, the difference in H_c between the silicon

and silicon oxide might be due to the different crystalline (Si) and amorphous (SiO₂) substrates that may affect the domain wall,^{44–48} meaning, the coercivity is associated with the change of grain size (D). It cannot be excluded that it can also be ascribed to the presence of the soft phase α-Fe with different percentages (Table I). Finally, the hysteresis loops of the Gd7 films confirm the tentative phase attribution that was done by XRD analysis since Gd7/Si displays significantly higher coercive field and saturation magnetization values than Gd7/SiO₂ consistent with the presence of L1₀ FePd and α-Fe.

It must be pointed out that the values of M_s are generally lower than expected and cannot be always explained with the available phase analysis. Indeed, in literature, it is reported that an antiferromagnetic coupling could appear between the Fe 3d and Gd 4f magnetic moments²⁸ as observed in Fe–Gd alloys^{49,50} and confirmed in Refs. 28, 29, and 31. Although we cannot directly assess the presence of such antiferromagnetic coupling, that would at least partially explain the observed reduction of M_s.

Finally, it is worth comparing the magnetic properties of the films where some Pd was replaced with Gd with those containing no Gd (last row of Table III and Refs. 17 and 51). An overall reduction in coercivity with increasing Gd content is observed, probably to be attributed to the fact that when some Pd is replaced with Gd there is an excess of Fe, and besides the hard L1₀ phase, the soft α-Fe phase is also formed.

The values of (BH)_{max} energy product are given in Table IV for the deposited and annealed films, and it is clear that the value of (BH)_{max} becomes maximum when the amount of Gd is 3% for both substrates. This dependence is strongly correlated to the similar trend displayed by H_c, as reported in Table III. This behavior is in line with the presence of a peak of H_c at intermediate

TABLE IV. Energy product (BH) max values of the as-deposited and annealed films.

Sample	(BH) _{max} (MGOe)			
	Si(100)		Si/SiO ₂	
	As-deposited	Annealed	As-deposited	Annealed
Fe ₅₆ Pd ₄₃ Gd ₁	2.13 × 10 ⁻⁶	0.0040	1.03 × 10 ⁻⁶	0.0025
Fe ₅₆ Pd ₄₁ Gd ₃	1.36 × 10 ⁻⁵	0.0073	1.27 × 10 ⁻⁵	0.0032
Fe ₅₆ Pd ₃₉ Gd ₅	5.27 × 10 ⁻⁶	8.03 × 10 ⁻⁵	1.16 × 10 ⁻⁶	1.86 × 10 ⁻⁴
Fe ₅₆ Pd ₃₇ Gd ₇	4.13 × 10 ⁻⁷	8.7 × 10 ⁻⁴	6.51 × 10 ⁻⁷	5.197 × 10 ⁻⁵

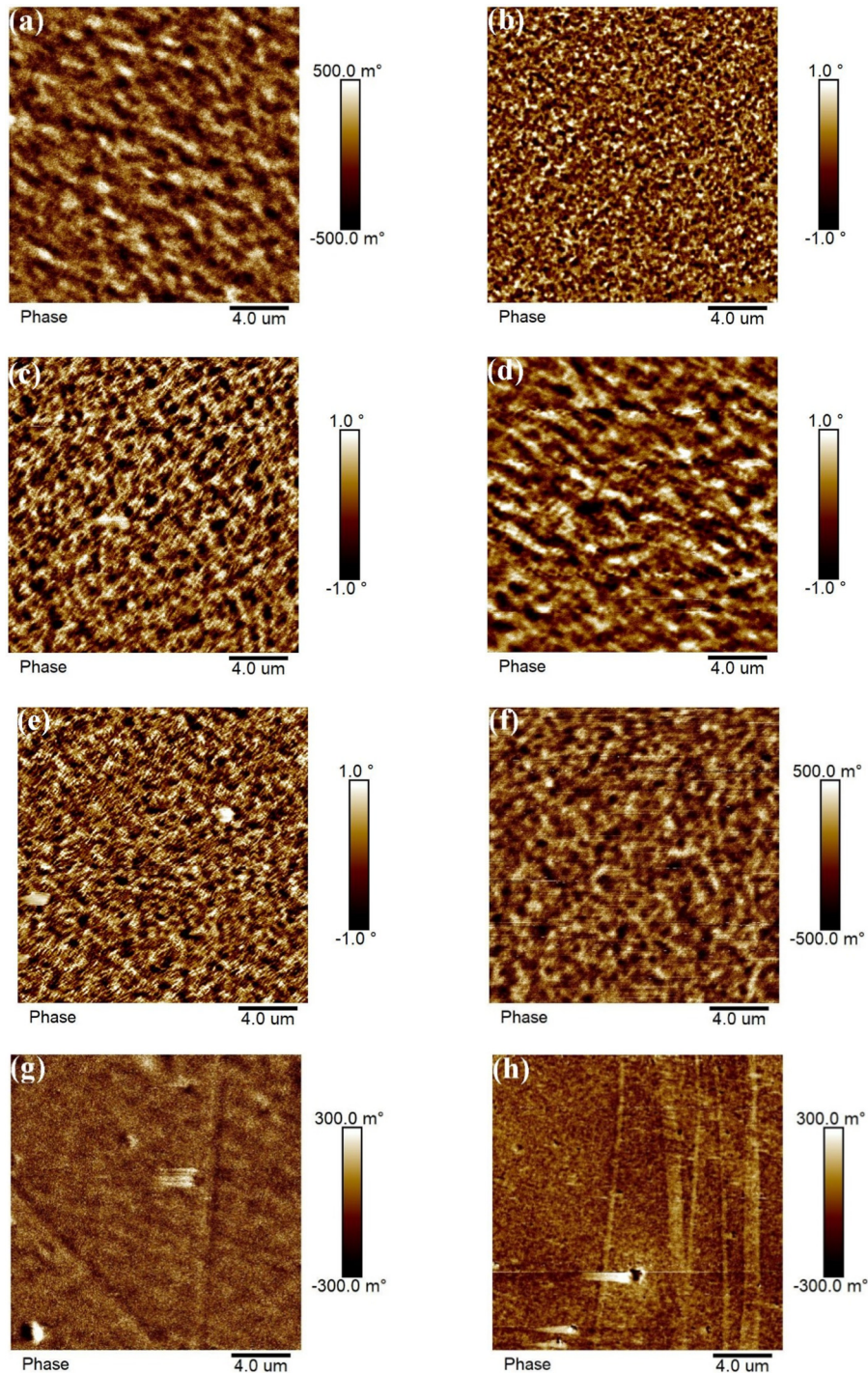


FIG. 9. MFM images of the $\text{Fe}_{56}\text{Pd}_{44-x}\text{Gd}_x$ films annealed at $530\text{ }^\circ\text{C}$ for 4h: (a) Gd1/Si, (b) Gd1/SiO₂, (c) Gd3/Si, (d) Gd3/SiO₂, (e) Gd5/Si, (f) Gd5/SiO₂, (g) Gd7/Si, and (h) Gd7/SiO₂.

11 November 2024 09:37:28

thickness; since at large thickness, the domain wall mobility is higher, and at lower thickness, the dominant process of magnetization reversal is rotations. Moreover, samples with Gd content other than 3% may have a soft-to-hard magnetic phase ratio relatively

shifted to the soft ones, as confirmed by the FORC analysis later, therefore leading to reduced $(\text{BH})_{\text{max}}$ values.

MFM was used to study the structure of the magnetic domains at their in-plane magnetic remanence. The MFM images

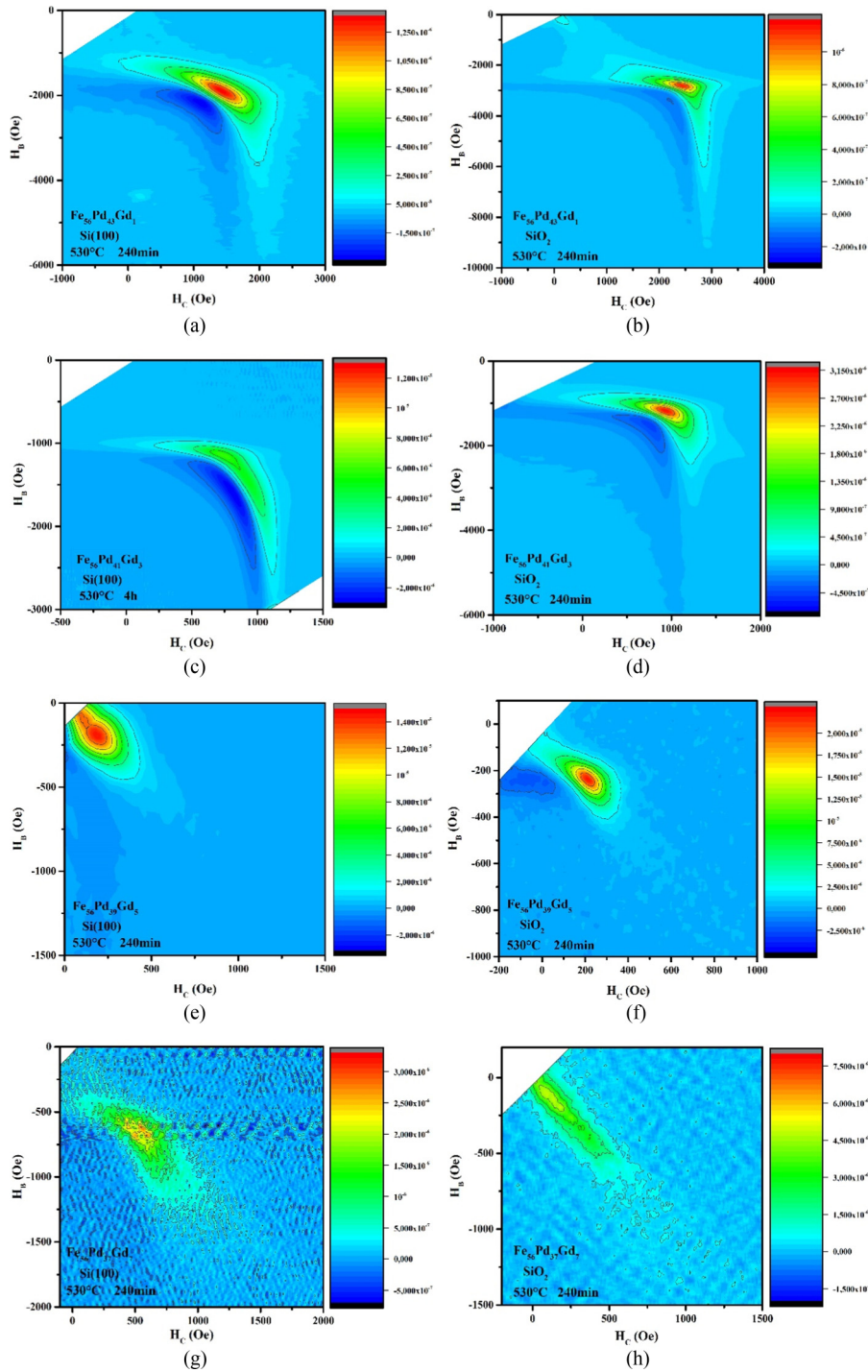


FIG. 10. FORC distribution in the (H_C, H_B) plane of the annealed $\text{Fe}_{56}\text{Pd}_{44-x}\text{Gd}_x$ films at 530°C for 4h: (a) Gd1/Si, (b) Gd1/SiO₂, (c) Gd3/Si, (d) Gd3/SiO₂, (e) Gd5/Si, (f) Gd5/SiO₂, (g) Gd7/Si, and (h) Gd7/SiO₂.

11 November 2024 09:37:28

of the annealed $\text{Fe}_{56}\text{Pd}_{44-x}\text{Gd}_x$ films deposited on Si and SiO₂ at 530°C for 4 h are reported in Fig. 9: all look very different from their counterparts of the as-deposited samples shown in Fig. 5. A complex multi-domain formation is observed in all films whether

deposited on Si or SiO₂ [Figs. 9(a)–9(f)], which strongly depends mainly on the microstructure and phases forming the film. The presence of the L1₀ FePd phase stimulates the formation of this complex configuration, thanks to its large magnetic anisotropy and

random crystal orientation in space, thus leading to a typical maze domain structure, intermediate between weak stripes and dense bubbles, possibly due to the increased domain wall energy associated to the increased domain wall width.⁵² The perpendicular component of the magnetization that appears in these films, with an irregular pattern, confirms the development of the $L1_0$ FePd phase having a c -axis randomly oriented; therefore, the local anisotropies are oriented in different directions in space. For the samples with higher Gd content, the reduced amount of the $L1_0$ phase, according to XRD, is reflected in the lower contrast of the MFM images (see the expansion of the color scale). The domains are characterized by a substantial difference in size that can be explained by the presence of magnetic coupling between two magnetic phases (hard and soft phases), which was studied through FORC measurements.

Figure 10 shows the FORC diagrams of the annealed $Fe_{56}Pd_{44-x}Gd_x$ thin films deposited on Si (left) and SiO_2 (right) in the (H_C , H_B) plane. The Gd1 films show a single peak for H_C and H_B values close to ≈ 2000 and 3000 Oe for Si and SiO_2 , respectively, that comes from the coercive fields' distribution of the harder magnetic phase ($L1_0$ FePd), but the dark blue halo besides the FORC peak indicates a strong coupling between the two hard/soft magnetic components ($L1_0$ FePd and α -Fe). By increasing the amount of Gd, the peak gradually becomes less severe, indicating a weaker irreversible magnetization reversal contribution [Figs. 10(e)–10(h)]. The dark blue negative halo started to disappear when the Gd amount increased to 5% and completely disappeared for Gd = 7%, indicating that the films contain a progressively more dominant soft phase (see Table I) and also pointing to the absence of magnetic interactions between the different magnetic phases, a result consistent with XRD data, MFM images, and (BH)max values.

The coherent picture arising from these microstructural and magnetic data allows us to further confirm the phases that were marked with a question mark in Table I.

IV. CONCLUSION

To study the effect of gadolinium on the structural and magnetic properties of the Fe–Pd system, $Fe_{56}Pd_{44-x}Gd_x$ ternary films were prepared by vacuum evaporation on Si(100) and Si/ SiO_2 substrates. Annealing at 530°C for 4h transformed the disordered fcc FePd phase into the ordered $L1_0$ FePd phase in films with lower content of Gd, with local anisotropies oriented randomly. On increasing the Gd content, the appearance of soft phases ($L1_2$ FePd, Fe_3O_4) after annealing leads to a reduction in the coercivity, as a consequence of a progressive reduction in the fct phase. Also M_s values are affected by the phases present in the film, in particular, by the soft phases. Overall, no major differences were observed in magnetic properties between the two kinds of substrates, whereas some silicide formation was observed only in the Si substrate with native oxide, indicating that the wafer coated with amorphous SiO_2 can be preferred over the Si one, which is more reactive with Pd during thermal treatments and, therefore, may lead to the formation of unwanted phases.⁴² FORC measurements show a single peak corresponding to the hard phase, with signs of the interaction between the soft and hard phases in the samples with lower Gd content.

In spite of the difficulty in assessing where Gd atoms distribute in the microstructure of these Fe–Pd–Gd thin films, a few

general conclusions can nonetheless be drawn: (i) the presence of Gd severely affects the thermal deposition process, leading to both a significantly reduced thickness and an unexpected Pd depletion; the mechanisms leading to this result are yet to be understood; (ii) Gd enters into the Fe and/or Fe–Pd phases, as a clear evolution of the magnetic properties with Gd content is observed; (iii) the choice of the substrate does not lead to significant variations of the measured properties, except that SiO_2 is less prone to forming Pd silicides during annealing; (iv) compared to the Fe–Pd system of similar composition (see Table III and Refs. 17 and 51), substituting some Pd with Gd leads to a weakening of the hard magnetic properties. Therefore, with this study, we have helped clarify the role of Gd in replacing some Pd in the Fe–Pd system. The difficulty in controlling the amount of rare earth during the deposition process and the reduction in the hard magnetic properties when the Gd content is increased seem to indicate that in this system the partial substitution of the precious metal with the rare earth element will negatively impact applications. It is, therefore, suggested that Fe, instead of Pd, could be partially replaced by Gd, in order to try to improve the hard magnetic properties of annealed samples. In conclusion, this study has contributed in understanding the so far almost unexplored Fe–Pd–Gd ternary system.

AUTHOR DECLARATIONS

Conflict of Interest

The authors have no conflicts to disclose.

Author Contributions

Mohamed Abdennour Sahari: Conceptualization (equal); Formal analysis (equal); Investigation (equal); Visualization (equal); Writing – original draft (equal); Writing – review & editing (equal). **Elena Sonia Olivetti:** Formal analysis (supporting); Investigation (supporting); Writing – review & editing (supporting). **Alessandro Magni:** Investigation (supporting). **Gianluca Fiore:** Investigation (supporting). **Mokhtar Boudissa:** Conceptualization (equal); Supervision (supporting). **Paola Tiberto:** Validation (equal); Writing – review & editing (supporting). **Saida Bahamida:** Conceptualization (equal); Supervision (supporting); Writing – review & editing (supporting). **Marco Coisson:** Supervision (equal); Writing – review & editing (equal).

DATA AVAILABILITY

The data that support the findings of this study are available from the corresponding author upon reasonable request.

REFERENCES

- 1 K. E. Knippling, D. C. Dunand, D. N. Seidman, and Z. Metallk, "Criteria for developing castable, creep-resistant aluminum-based alloys—A review," *Int. J. Mater. Res.* **97**, 246 (2022).
- 2 V. K. Pecharsky and K. A. Gschneidner, Jr., "Magnetocaloric effect and magnetic refrigeration," *J. Magn. Magn. Mater.* **200**, 44–56 (1999).
- 3 K. Matsumoto, K. Asamoto, Y. Nishimura, Y. Zhu, S. Abe, and T. Numazawa, "Magnetocaloric effect of RM_2 (R = rare earth, M = Ni, Al) intermetallic compounds made by centrifugal atomization process for magnetic refrigerator," *J. Phys.: Conf. Ser.* **400**, 052020 (2012).

- ⁴K. Aledealat, B. Aladerah, A. Obeidat, and A. M. M. Rawashdeh, "Enhancing the performance of rare-earth free permanent magnets: A computational study of nitrogen and oxygen defects in CoPt, CoFePt₂, and CoNiPt₂ alloys," *J. Phys. Chem. Sol.* **183**, 111649 (2023).
- ⁵A. Rebei and J. Hohlfield, "The magneto-optical Barnett effect: Circularly polarized light induced femtosecond magnetization reversal," *Phys. Lett. A* **372**, 1915–1918 (2008).
- ⁶D. K. Hairston and M. H. Kryder, "The TM dependence of the magneto-optic signal in GdTb-TM thin films," *J. Appl. Phys.* **63**, 3621–3623 (1988).
- ⁷T. Yang, T. Matsumoto, H. Yamane, M. Kamiko, and R. Yamamoto, "Perpendicular magnetic anisotropy and magneto-optical properties of (Co-Tb)/Pd multilayers," *J. Magn. Magn. Mater.* **198–199**, 357–359 (1999).
- ⁸B. Zhou, Y. Liu, S. Li, W. Fan, X. Liao, J. He, H. Yu, and Z. Liu, "Phase precipitation and magnetic properties of melt-spun ternary Gd₂Fe₁₄B alloy and advantages of gadolinium substitution in Y₂Fe₁₄B alloy," *J. Rare Earths* **41**, 1058–1067 (2023).
- ⁹M. Senthil Kumar, "Temperature dependence of magnetization in Fe–Pd thin films," *Mater. Sci. Eng. B* **162**, 59–63 (2009).
- ¹⁰S. Bahamida, A. Fnidiki, A. Laggoun, and A. Guittoum, "A comparative structural and magnetic study of Fe_{100-x}Pd_x (x = 15, 20 and 36) thin films deposited on Si (100) and glass substrates," *J. Magn. Magn. Mater.* **392**, 139–147 (2015).
- ¹¹T. Sakamoto, T. Fukuda, T. Kakeshita, T. Takeuchi, and K. Kishio, "Magnetic field-induced strain in iron-based ferromagnetic shape memory alloys," *J. Appl. Phys.* **93**, 8647 (2003).
- ¹²R. D. James and M. Wuttig, "Magnetostriction of martensite," *Philos. Mag. A* **77**, 1273 (1998).
- ¹³Y. Furuya, N. W. Hagood, H. Kimura, and T. Watanabe, "Shape memory effect and magnetostriction in rapidly solidified Fe-29.6 at% Pd alloy," *Mater. Trans. JIM* **39**, 1248 (1998).
- ¹⁴Y. Ma, M. Zink, and S. G. Mayr, "Biocompatibility of single crystalline Fe₇₀Pd₃₀ ferromagnetic shape memory films," *J. Appl. Phys.* **96**, 213703 (2010).
- ¹⁵J. R. Hatrick-Simpers, C. Jun, M. Murakami, A. Orozco, L. Knauss, R. J. Booth, E. W. Greve, S. E. Lofland, M. Wuttig, and I. Takeuchi, "High-throughput screening of magnetic properties of quenched metallic-alloy thin-film composition spreads," *Appl. Surf. Sci.* **254**, 734–737 (2007).
- ¹⁶E. Burz and P. Vlaic, "Magnetic properties of iron-palladium solid solutions and compounds," *J. Optoelectron. Adv. Mater.* **12**, 1869–1878 (2010).
- ¹⁷S. Bahamida, A. Fnidiki, M. Coisson, G. Barrera, F. Celegato, E. S. Olivetti, P. Tiberto, and M. Boudissa, "Effect of the A1 to L10 transformation on the structure and magnetic properties of polycrystalline Fe₅₆Pd₄₄ alloy thin films produced by thermal evaporation technique," *Thin Solid Films* **668**, 9–13 (2018).
- ¹⁸G. D. Yıldız, "Intersection magnetization and temperature revealed by FCC-FCT phase transformation in the FePd binary alloy system," *J. Supercond. Novel Magn.* **33**, 2051–2058 (2020).
- ¹⁹P. V. Jasen, E. A. Gonzalez, N. J. Castellani, and A. Juan, "Theoretical study of hydrogen adsorption on FePd face-centered cubic alloy surfaces," *Phys. Rev. B* **71**, 235422 (2005).
- ²⁰K. J. Bryden and J. Y. Ying, "Electrodeposition synthesis and hydrogen absorption properties of nanostructured palladium-iron alloys," *Nanostruct. Mater.* **9**(5), 485–488 (1997).
- ²¹F. M. Takata, G. Pattanaik, W. A. Soffa, P. T. A. Sumodjo, and G. Zangari, "Synthesis of L10 Fe-Pd films by electrodeposition and thermal annealing," *Electrochem. Commun.* **10**, 568–571 (2008).
- ²²V. Gehanno, A. Marty, B. Gilles, and Y. Samson, "Magnetic domains in epitaxial ordered FePd(001) thin films with perpendicular magnetic anisotropy," *Phys. Rev. B* **55**, 12552–12555 (1997).
- ²³L. Wang, Z. Fan, A. G. Roy, E. David, and E. D. Laughlin, "Effects of atomic ordering on the curie temperature of FePd L10L10 type alloys," *J. Appl. Phys.* **95**, 7483–7485 (2004).
- ²⁴J. Cui and R. D. James, "Study of Fe/sub 3/Pd and related alloys for ferromagnetic shape memory," *IEEE Trans. Magn.* **37**, 2675–2677 (2001).
- ²⁵J. Cui, T. W. Shield, and R. D. James, "Phase transformation and magnetic anisotropy of an iron-palladium ferromagnetic shape-memory alloy," *Acta Mater.* **52**, 35–47 (2004).
- ²⁶J. J. Huo, Y. S. Du, G. Cheng, X. F. Wu, L. Li, Z. C. Xia, and G. H. Rao, "Experimental investigation of the isothermal section in Fe-Gd-Pd ternary system at 873 K," *J. Phase Equilib. Diffus.* **39**, 152–165 (2018).
- ²⁷X. L. Chen, J. Wang, T. L. Chen *et al.*, "Thermodynamic re-assessment of the Fe-Gd and Fe-Sm binary systems," *Calphad* **58**, 151–159 (2017).
- ²⁸W. Zhang, S. Jiang, P. K. J. Wong, L. Sun, Y. K. Wang, K. Wang, M. P. Jong, W. G. Wiel, G. Laan, and Y. Zhai, "Engineering Gilbert damping by dilute Gd doping in soft magnetic Fe thin films," *J. Appl. Phys.* **115**, 17A308 (2014).
- ²⁹H. Y. Zhang, J. T. Ouyang, D. Ding, H. L. Li, J. G. Wang, and W. H. Li, "Influence of Fe substitution on thermal stability and magnetocaloric effect of Gd₆₀Co_{40-x}Fe_x amorphous alloy," *J. Alloys Compd.* **769**, 186–192 (2018).
- ³⁰Y. Fu, L. Sun, J. S. Wang, X. J. Bai, Z. X. Kou, Y. Zhai, and H. R. Zhai, "Magnetic properties of (Ni₈₃Fe₁₇)_{1-x}Gd_x thin films with diluted Gd doping," *IEEE Trans. Magn.* **45**(10), 4004–4007 (2009).
- ³¹N. Schmidt, (2020). FePt-based thin films: doping with 3d and 4f elements.
- ³²Z. Khan, "Influence of gadolinium on the microstructure and mechanical properties of steel and stainless steel," *J. South. Afr. Inst. Min. Metall.* **112**(4), 309–321 (2012), <https://www.saimm.co.za/journal/v112n04p309.pdf>.
- ³³M. Yang, Z. Zhang, Y. Liu *et al.*, "Corrosion and mechanical properties of AM50 magnesium alloy after modified by different amounts of rare earth element gadolinium," *Open Phys.* **14**(1), 444–451 (2016).
- ³⁴P. Scherrer, *Göttinger. Nachrichten.* **2**, 98 (1918), <http://eudml.org/doc/59018>.
- ³⁵J. Laigo, F. Christien, R. Le Gall, F. Tancret, and J. Furtado, "SEM, EDS, EPMA-WDS and EBSD characterization of carbides in HP type heat resistant alloys," *Mater. Charact.* **59**, 1580–1586 (2008).
- ³⁶R. Vaia, M. Weathers, and W. Bassett, "Anomalous peaks in grazing incidence thin film X-ray diffraction," *Powder Diff.* **9**(1), 44–49 (1994).
- ³⁷J. Hintermayr, N. Y. Safonova, A. Ullrich, and M. Albrecht, "Magnetic properties and structure of Gd-implanted L 10 FePt thin films," *AIP Adv.* **9**, 055020 (2019).
- ³⁸J. Liu, Q. Wang, M. Wu, Y. Zhang, H. Shen, and W. Ma, "Improving the refrigeration capacity of Gd-rich wires through Fe-doping," *J. Alloys Compd.* **711**, 71–76 (2017).
- ³⁹Z. Wu, X. a. Fan, G. Li, Z. Gan, J. Wang, and Z. Zhang, "Evolution from amorphous to nanocrystalline and corresponding magnetic properties of Fe–Si–B–Cu–Nb alloys by melt spinning and spark plasma sintering," *Mater. Sci. Eng. B* **187**, 61–66 (2014).
- ⁴⁰R. Gopalan, A. Kündig, M. Ohnuma, S. Kishimoto, and K. Hono, "Mechanically milled and spark plasma sintered FePt-based bulk magnets with high coercivity," *Scr. Mater.* **52**, 761–765 (2005).
- ⁴¹L. B. Freund and S. Suresh, *Thin Film Materials, Stress, Defect Formation and Surface Evolution* (University Press, Cambridge, 2004).
- ⁴²P. Tiberto, G. Barrera, F. Celegato, M. Coisson, E. S. Olivetti, and F. Vinai, "Microstructural evolution and magnetic properties in Fe₅₀Pd₅₀ sputtered thin films submitted to post-deposition annealing," *J. Alloys Compd.* **615**, S236–S241 (2014).
- ⁴³M. L. Lwin, D.-w. Shin, S. W. Nam *et al.*, "Effect of single and co-addition of rare earth on the microstructure, mechanical properties, and corrosion behavior of AZ31 magnesium alloys," *J. Mater. Eng. Perform.* (published online 2023).
- ⁴⁴W. Li, T. Ohkubo, and K. Hono, "Effect of post-sinter annealing on the coercivity and microstructure of Nd-Fe-B permanent magnets," *Acta Mater.* **57**, 1337–1346 (2009).
- ⁴⁵Y. Nakamura, "Effect of quenched-in vacancies on the weak magnetization of nickel," *J. Phys. Soc. Jpn.* **16**, 2167–2171 (1961).
- ⁴⁶L. Néel, "Thermoremanent magnetization of fine powders," *Rev. Mod. Phys.* **25**, 293 (1953).
- ⁴⁷L. Néel, "Magnétisme-le champ coercitif d'une poudre ferromagnétique cubique A grains anisotropes," *C. R. Hebd. Seances Acad. Sci.* **224**, 1550–1551 (1947).

⁴⁸X. A. Fan, Z. Y. Wu, G. Q. Li, J. Wang, Z. D. Xiang, and Z. H. Gan, "High resistivity and low core loss of intergranular insulated Fe-6.5 wt.% Si/SiO₂ composite compacts," *Mater. Design* **89**, 1251–1258 (2016).

⁴⁹M. Mansmann and W. E. Wallace, *J. Chem. Phys.* **40**, 1167 (1964).

⁵⁰P. Hansen, C. Clausen, G. Much, M. Rosenkranz, and K. Witter, *J. Appl. Phys.* **66**, 756 (1989).

⁵¹S. Bahamida, A. Fnidiki, M. Coisson *et al.*, "Role of structural defects on the magnetic properties of annealed Fe₅₆Pd₄₄ thin films upon development of the ordered L10 phase," *J. Magn. Mag. Mater.* **563**, 169991 (2022).

⁵²S. Bahamida, A. Fnidiki, M. Coisson, A. Laggoun, G. Barrera, F. Celegato, and P. Tiberto, "Mixed exchange-coupled soft α -(Fe₈₀Pd₂₀) and hard L10FePd phases in Fe₆₄Pd₃₆ thin films studied by first order reversal curves," *Mater. Sci. Eng. B* **226**, 47–56 (2017).